Dynamic Analysis of a Reinforced Concrete Structure Using Plasticity and Interface Damage Models

I. Rhee, K.J. Willam, B.P. Shing,
University of Colorado at Boulder

ABSTRACT: This paper examines the global and local behavior of a five-story lightly reinforced concrete shear-wall structure subjected to seismic loading in two directions on a shaking table. Results of the shaking table tests conducted under CAMUS 2000-1 are used as a reference to assess the performance of damage and elasto-plastic finite element simulations in the time domain.

Keywords: dynamic earthquake response, five-story shear-wall structure, 2-D shaking table experiments, damage and plastic concrete models, interface damage elements

1 INTRODUCTION

In 1998 a combined experimental and numerical research program CAMUS was launched in France with the aim of evaluating the effects of 2-D earthquake motions and torsion on lightly reinforced concrete shear wall structures. As part of the program, two 1:3-scale structural models representative of a five-story reinforced concrete building (Fig. 1) were tested on the Azalee shaking table of the Commissariat a l'Energie Atomique (CEA) in the Saclay Nuclear Center. The first structure (CAMUS 2000-1) was subjected to horizontal bi-directional excitation. A combination of table accelerations was applied at three levels of amplitude (the nominal accelerations were 0.15g, 0.40g and 0.55g in RUN1, RUN2, RUN3). Structural stiffness was provided by two identical shear walls in one direction, and a steel bracing system in the orthogonal direction. For the second test (CAMUS 2000-2), an in-plane excitation was applied to two shear walls of different geometry introducing torsional response due to lack of symmetry[1][2].

2 GEOMETRIC MODELING

The basic geometry and the mesh layout of the 3-D finite element model of the CAMUS 2000-1 test article are illustrated in Figures 1 and 2. The main difficulty of the geometric idealization was the transverse bracing model of the hat frame at each story, which determines the interaction between the two shear walls under transverse excitation.

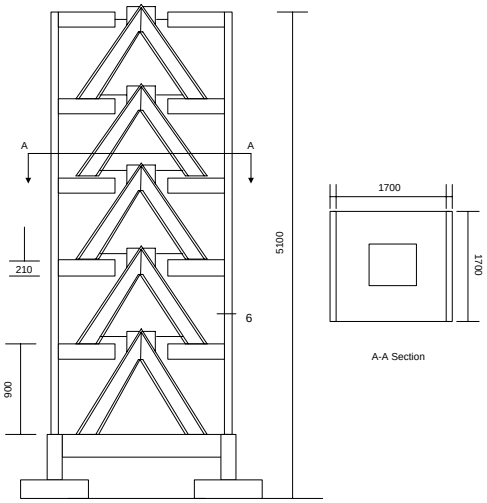

Figure 1. Five-story shear wall building : Layout of specimen

In the 3-D finite element model, the transverse hat frame was replaced by the rectangular solid frame structure shown in Figure 3(a), the stiffness of which was calibrated from the frequency measured

in the experiment, see Table 1. The 3-D finite element mesh consists of TETRA elements (38,400 four-node tetrahedrons) which are arranged in four layers through the wall thickness in the form of union-jack triangulation. In addition, BRICK8 elements (1,100 eight-node bricks) are used for the shaking table, the floor slabs between the two walls, and the transverse bracing system. Finally, BAR3D elements (562 two-node bars) are used for the vertical reinforcement and the horizontal stirrups. The 3-D finite element mesh has a total of 13,517 nodes (39,906 dofs) and 46,926 elements as shown in Figures 2 and 3. A total mass of 60 tons is added to the five floors with 12 tons lumped at each story. The shear wall structure stands on the rigid shaking table which has 40% of the total mass. A total of four springs are used to model the support of the shaking table. The spring constants are 215 MN/m each.

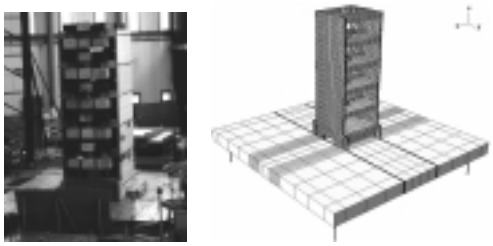

(a) (b)

Figure 2. Five-story shear wall building : (a) Experimental setting by courtesy of [2], (b) 3-D finite element mesh.

3 LINEAR DYNAMIC ANALYSIS

3.1 *Frequencies for Tuning Elastic Damage*

The purpose of this task is to develop an equivalent linear model which is representative of a simplified engineering approach. For concrete, the nominal value of Young's modulus E_c=28,000 MPa was specified by the CAMUS test program, and for steel, E_s=200,000 MPa. Poisson ratios of concrete and steel were given to be $\nu = 0.2$ and $\nu = 0.3$ respectively. If these nominal elastic material values are used in the 3-D finite element model, the first three frequencies (1st mode: Out-of-Plane Bending, 2nd mode: In-Plane Bending, 3rd mode: Torsion as shown in Figure 4.) are considerably higher than those measured in the experiment under low amplitude excitation (before testing), see summary in Table 1. The intent of the equivalent linear dynamic analysis is to tune the frequencies of the 3-D model by reducing the Young modulus of concrete due to damage in the 1st floor, see Table 2.

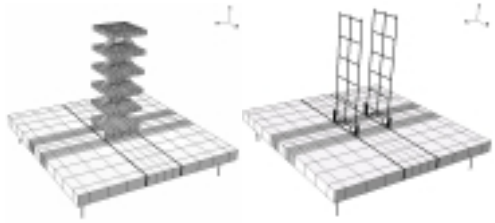

(a) (b)

Figure 3. Five story shear wall building:(a) Transverse floor and bracing system, (b) Reinforcements of shear walls.

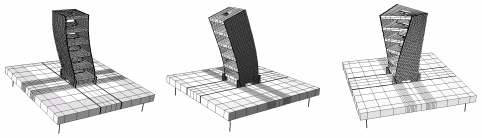

(a) (b) (c)

Figure 4. First three eigenmodes of CAMUS III structure: (a) Out-of-Plane, (b) In-Plane, (c) Torsion modes.

Table 1: Experimental frequencies before testing

TEST #	1st Mode	2nd Mode	3rd Mode
RUN1	5.80 Hz	6.25 Hz	11.6 Hz
RUN2	5.40 Hz	6.00 Hz	11.0 Hz
RUN3	4.20 Hz	5.80 Hz	10.4 Hz
NOMINAL	6.28 Hz	9.28 Hz	15.1 Hz

Table 2: Experimental frequencies after testing

TEST #		1st Mode	2nd Mode	3rd Mode
RUN1	E	4.00 Hz	4.39 Hz	10.2 Hz
	T	4.76 Hz	4.97 Hz	9.80 Hz
RUN2	E	4.00 Hz	4.39 Hz	8.10 Hz
	T	4.04 Hz	4.34 Hz	7.96 Hz
RUN3	E	2.93 Hz	2.73 Hz	6.40 Hz
	T	3.05 Hz	3.78 Hz	6.29 Hz

*E: Measured, T:Tuned (elastic concrete damage of 1st floor)

Experimental observations indicate that the main damage caused by localized cracking and global degradation developed mainly in the 1st floor of the two shear walls. In other words, a simple engineering approach assumes uniform damage in the 1st floor of the two shear walls with a damage parameter d=1-E_d/E_o = 0.94 to 0.98. This elastic

degradation is used subsequently in the equivalent linear dynamic response analysis including proportional damping. Three ground motions with different levels of acceleration (0.15g, 0.40g, 0.55g) are applied at the base of the shaking table. To emulate the experimental condition, the base displacements at the table are used to input the earthquake motion rather than the accelerations measured at the transducers shown in Figure 7. The displacement histories in Figure 5 and 6 are applied simultaneously in the two directions `in-plane' and `out-of-plane' to the two shear walls shown in Figure 7.

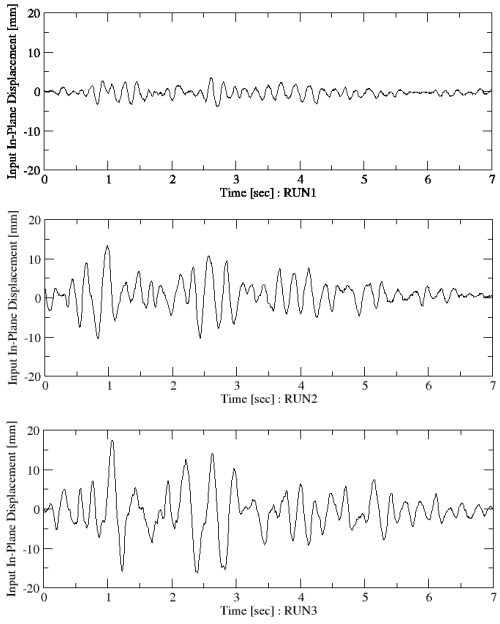

Figure 5. In-Plane displacement input: RUN1,RUN2, RUN3

3.2 *Linear Dynamic Response of Partially Damaged Structure*

The main results of the elastic damage analyses are shown in Figure 8 and 9. Although the eigen-frequencies of the structure in each RUN are pre-determined by tuning experimental data, the global behavior under bi-axial seismic loading depends primarily upon the level of damage in the 1st floor of the two shear walls where the large base shears and moments are expected. There are two main issues for this type of analysis, the amplitudes and the frequencies of the response histories. The amplitudes are primarily influenced by the amount of viscous Rayleigh damping assuming 2% proportional damping applied to the 1st and 3rd modes. The frequencies shift due to the large reduction of elastic stiffness of the two concrete walls in the damaged 1st floor (RUN1: E_c=2,000 MPa, RUN2: E_c=1,000 MPa, RUN3: E_c=500 MPa from the initial intact value E_o=28,000 MPa) as described in Section 3.1.

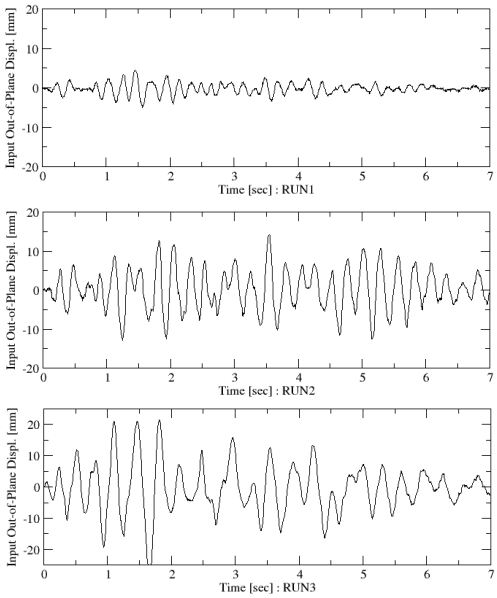

Figure 6. Out-of-Plane displacement input: RUN1, RUN2, RUN3

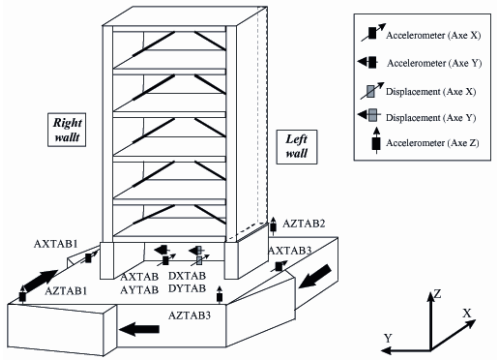

Figure 7. Bi-seismic excitation of shaking table : In-Plane and Out-of-Plane directions by courtesy of [2].

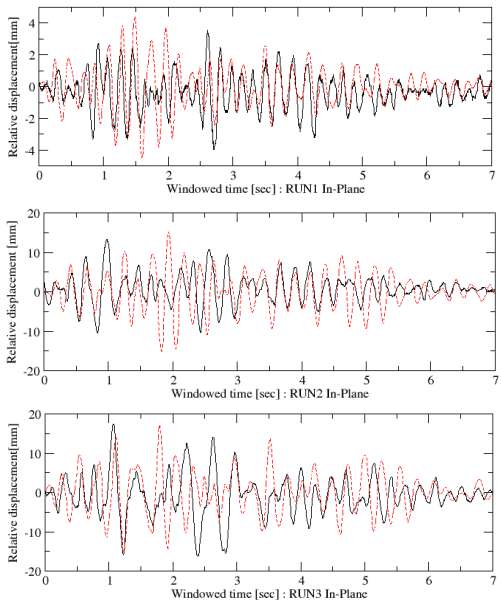

Figure 8. Relative in-plane displacement histories: RUN1, RUN2, RUN3.

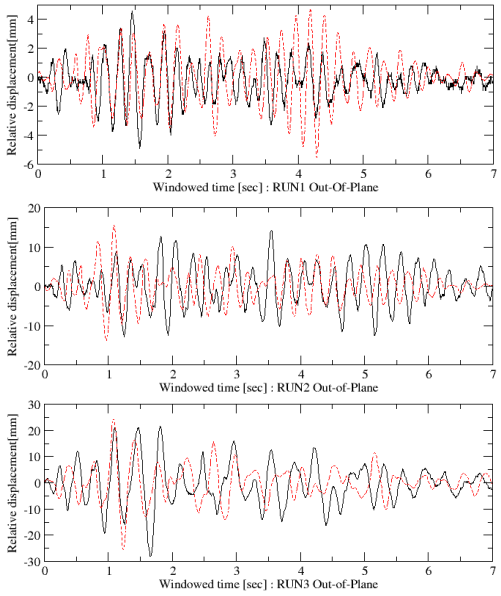

Figure 9. Relative out-of-plane displacement histories: RUN1, RUN2, RUN3.

4 NONLINEAR PUSH-OVER STUDY

4.1 *Material Nonlinearities in Concrete & Steel*

In view of the complex 3-D finite element model a simple material model is used for the inelastic behavior of reinforced concrete under cyclic loading. This model is based upon plasticity theory for concrete assuming associated flow with no hardening/softening. For the yield condition a parabolic Drucker-Prager condition is employed which permits an analytical solution of the plastic return map of the trial overstress in Eq. 1 as depicted in Figure 10.

$$F(\boldsymbol{\sigma}) = J_2 + \alpha I_1 - \beta = 0$$
$$F(\boldsymbol{\sigma}_{n+1}) = F(\boldsymbol{\sigma}_n + \mathbf{E} : \Delta\boldsymbol{\varepsilon} - \Delta\lambda \mathbf{E} : \mathbf{m}) = 0$$

where,

$$\alpha = (f_c^{'} - f_t^{'})/3, \quad \beta = (f_c^{'} \times f_t^{'})/3 \qquad (1)$$
$$\mathbf{m} = \partial F / \partial \sigma$$

Here f'_c and f'_t denote the uniaxial compressive and tensile strength values of concrete. When the yield surface is reached in tension, a crack is created perpendicularly to the major principal direction of stress, whereby its orientation rotates with the principal axis according to the isotropic (rotating) crack concept. The cyclic behavior of concrete in tension-compression under increasing amplitude is illustrated in Figure 11 (considering no softening takes place at the material level of observation during progressive cracking and crushing the hysteretic energy dissipation is overestimated significantly). For the axial behavior of the reinforcing steel bars an isotropic hardening plasticity model is adopted which results in the cyclic response behavior shown in Figure 12.

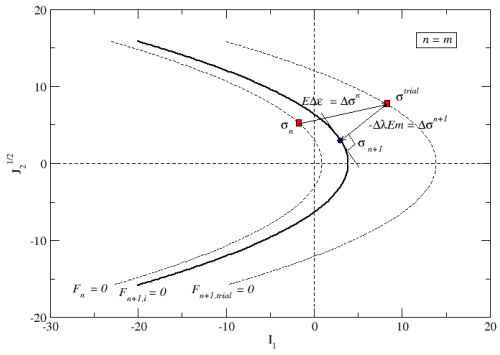

Figure 10. Plastic return map to parabolic Drucker-Prager loading surface.

The identification of the material parameters is quite simple. The nominal values of material properties are directly taken from the CAMUS 2000-1 test data. For steel, the elastic modulus is E_s = 200,000 MPa, the yield stress is f_y = 664 MPa, the failure stress is f_u = 733 MPa at 2.2% strain. For concrete, the initial elastic modulus is E_c= 28,000 MPa, the uniaxial compressive strength is f'_c = 35 MPa, and the direct tensile strength is f'_t = 3.5 MPa.

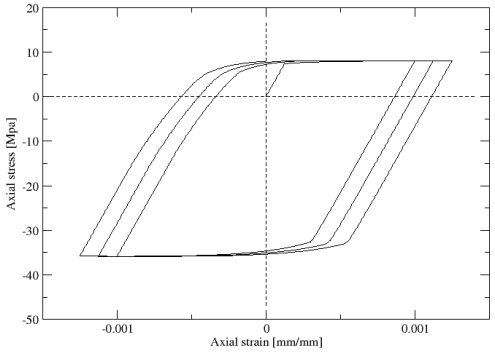

Figure 11. Cyclic uniaxial behavior of plain concrete in tension-compression.

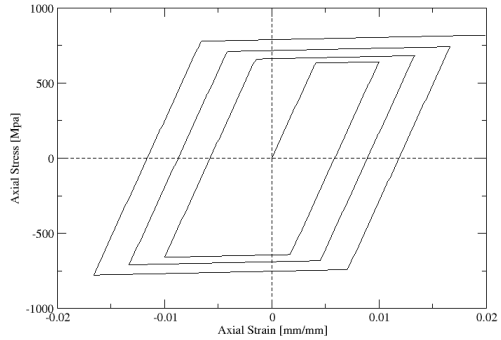

Figure 12. Cyclic uniaxial behavior of steel reinforcement.

4.2 *Static Nonlinear Push-Over Tests*

To appreciate the structural performance of the test article, a uniformly distributed horizontal displacement is applied at the top floor in the in-plane and out-of-plane directions. The main results of the monotonic push-over test are shown in Figure 13. The response predictions indicate that the elastic stiffness of this structure is quite similar for both in-plane and out-of-plane loading. Moreover, the level of RUN1 excitation is still in the linear elastic range, while the increased level of excitation of RUN2 and RUN3 indicate significant nonlinearities. Due to the linearity of the transverse bracing system and the floor connections between the two shear walls, the nonlinear effect of the out-of-plane response is relatively small since it is considerably below the ultimate load capacity F_P =789 kN when tensile cracking is confined to the 'narrow' wall region. In contrast, the nonlinear in-plane behavior is pronounced because of the perfectly-plastic Drucker-Prager concrete model. In this case confinement effects together with the associated flow rule overestimate the ultimate load capacity F_P =261 kN of the in-plane resistance according to elementary beam theory.

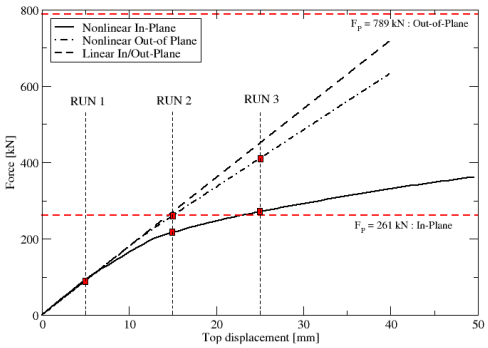

Figure 13. Force-relative displacement response under monotonically increasing in-plane displacement at top level.

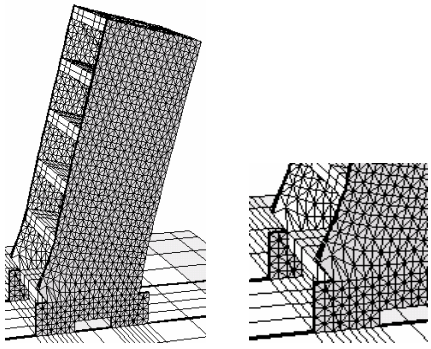

Figure 14. Deformed mesh of push-over test (in-plane failure mode).

5 NONLINEAR DYNAMIC ANALYSIS

The numerical simulations are performed using the general-purpose finite element program MFEM developed by a team in Aerospace Engineering Science at the University of Colorado at Boulder. To predict the inelastic seismic response of the tested structure with sufficient accuracy, special care is exercised to take into account all necessary geometric characteristics, construction details, reinforcement and boundary conditions. Assuming 0.5% critical damping for the first and third vibration mode, the damping parameters α and β are calculated for proportional Rayleigh damping, $\mathbf{C}= \alpha \mathbf{M}+ \beta \mathbf{K}$, where **M** and **K** are the structural mass and stiffness matrices. In view of the fact that the proportional damping characterization is consistent only for linear elastic systems, the damping matrix **C** is assumed to remain constant throughout the loading history. With increasing levels of excitation in RUN1, RUN2, and RUN3, the fundamental frequencies decrease due to concrete `cracking' and reinforcement yielding, which leads to considerable hysteretic damping of the lower structural modes. In contrast, viscous damping can only partially compensate for the different sources of hysteretic damping, unilateral closure, shear slip between the crack lips, bond slip between steel and concrete, etc. To solve the nonlinear equilibrium equations, the Newmark constant acceleration method (β =0.5 and γ =0.25) is used for the dynamic shaking table simulations. The nonlinear analysis results are shown in Figure 15 and 16. From the previous observation of the nonlinear push-over response in Figure 13, the behavior under RUN1 loading is still in the linear elastic regime. Note the experimental response closely agrees with the results of the nonlinear analysis using 0.5% damping and nominal (high) values for the elastic modulus of concrete.

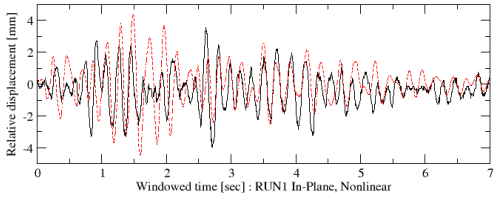

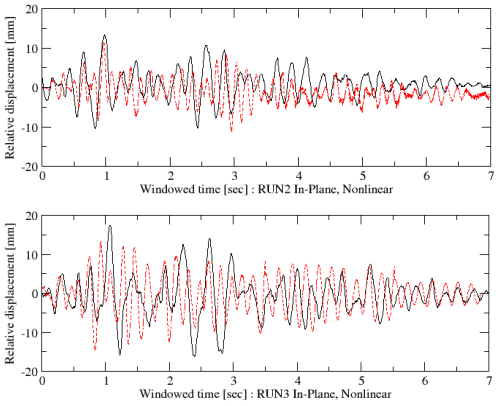

Figure 15. Relative In-Plane displacement response histories: RUN1-3, Nonlinear Analysis.

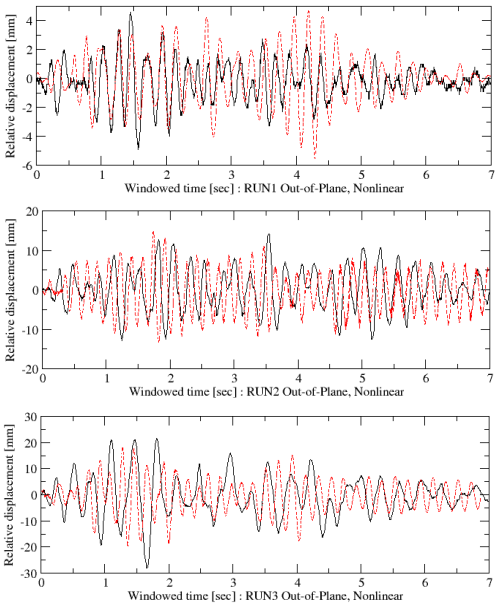

Figure 16. Relative Out-of-Plane displacement response histories: RUN1-3, Nonlinear Analysis.

FFT analysis of the experimental and computational response for RUN2 and RUN3 indicates that the frequencies of the elasto-plastic results are approximately 1.0 Hz higher than those of the experiments. However one should keep in mind that failure of the connections of the transverse bracing system with the floor slabs was observed during the experiments. Since the finite element model assumes linear elastic behavior of the floor and bracing connections the higher

frequencies may be caused by these modeling discrepancies.

6 INTERFACE DAMAGE MODEL IN 2-D

6.1 *Interface Models in Reinforced Concrete*

The tensile weakness of concrete and the ensuing cracking is a major factor contributing to the nonlinearity of reinforced concrete structures. There are four major approaches for describing this cracking in finite element analysis. They are (a) smeared (distributed) crack models, (b) embedded crack models, (c) discrete crack (cohesive) models, (d) fracture mechanics models. In the discrete crack model, the 'potential' failure zones are spread over the entire finite element domain with initial zero-thickness interface elements interspersed among elastic solid elements. When the interface element is subjected to mixed mode failure, the 'potential' crack candidates can be opened or slide according to the underlying softening law. For those problems that involve a few dominants cracks, the discrete crack model offers a realistic representation of those failure modes, that represent a strain or rather `displacement discontinuity', while the stress or rather traction boundary conditions remain nearly continuous. In addition, aggregate interlock and bond slip in mono- and bi-materials can be represented by this discrete cracking model although these physical issues are closely related to the mesh topology. The viewpoint of the discrete cohesive model is still a macroscopic one, with the basic behavior characteristics lumped in the elements. Therefore, an interface element has their life of its own in the elastic body. With cracking passing along element boundaries, the use of simplex elements such as the constant strain triangular (CST) element is well suited to concept and application in Figure 17. However, the interface elements do not adapt to sharp strain gradients except with a fine mesh. The stresses in the vicinity of the crack tip are mesh-dependent because of local stress concentrations.

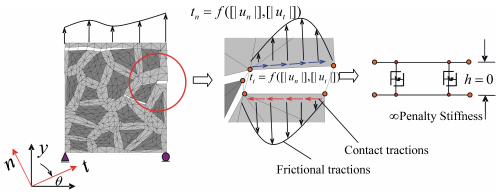

Figure 17. 2-D interface damage element.

6.2 *Cohesive Interface Formulation*

The material separation and thus damage of the structure is described by cohesive interface elements. Thereby, adjacent continuum elements are not damaged in this approach. Using this technique, the behavior of the material is split into two parts, the damage-free continuum with elastic material behavior that can vary across the body, and the interspersed cohesive interface zones between continuum elements, which represent localized damage of the material. The interface elements open up when damage occurs and entirely loose their stiffness at failure so that neighboring continuum elements are disconnected. For this reason, the crack can propagate only along the boundaries of solid elements in the form of inter-element failure. If the crack propagation direction is not known in advance, the mesh generation has to be sufficiently refined such that different crack interface paths are possible. The separation of the cohesive interfaces is calculated from the displacement jump $[|\mathbf{u}|]$, i.e. the difference between the displacements in adjacent continuum elements,

$$[|\mathbf{u}|] = \mathbf{u}^{+} - \mathbf{u}^{-}$$
$$[|u|] = \sqrt{[|u|]_n^2 + \alpha[|u|]_t^2} \qquad (2)$$

Rather than the defining the separation vector in global coordinates it is described in a local coordinate system to distinguish between normal separation, $[|u|]_n$, and tangential slip, $[|u|]_t$ in Eq. (2). The critical separation parameters denoted as $[|u|]_0$, and $[|u|]_f$ are defined in Figure 18. The maximum traction T_0, is a fracture parameter, which designates the 'cohesive strength' and is the value of the traction at $[|u|]_0$ while T_0 describes the maximum value of the traction separation relation $T([|u|])$. In the following, the exponential cohesive interface law shown in Figure 18 is used for the nonlinear interface simulations shown in Figures 19 and 20.

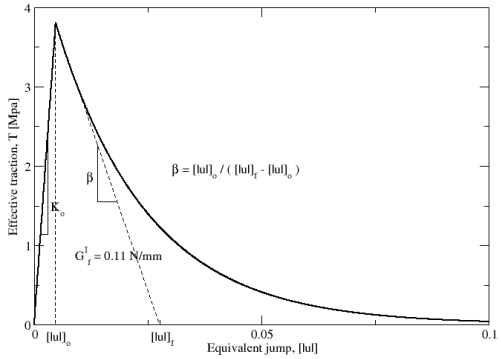

Figure 18. General softening law for the concrete cracking.

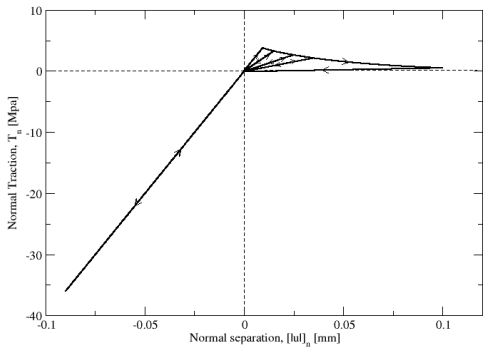

Figure 19. Normal behavior of 2-D interface element under tension-compression cycles.

$$T([|u|]) = T_o \exp^{\beta\left(1-\frac{[|u|]}{[|u|]_o}\right)}$$
$$\beta = \frac{[|u|]_o}{[|u|]_f - [|u|]_o} \qquad (3)$$

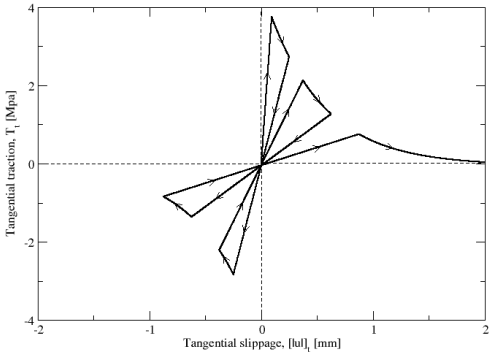

Figure 20. Cyclic shear behavior of 2-D interface element.

6.3 *Finite Interface Model of Push-Over Study*

In spite of using a simple method of placing interface elements among all solid elements, and in spite of the lack of generality in possible crack directions, a structured 'union-jack' mesh is used in this study. Hence, all possible crack directions are limited to horizontal, vertical and ± 45-degree diagonal directions. A total of 24,373 nodes (48,746 dofs), 22,976 elements (CST: 7,696, INT2D: 11,385, BAR2D: 3,894) are used in the deformed 2-D mesh shown in Figure 21. The same dimension and material parameters of CAMUS 2000-1 are used as in the previous analysis. Two types of interface elements are introduced to capture the nonlinearities of reinforced concrete. They are concrete-concrete interfaces (C-C) and concrete-steel interfaces (C-S). The former are essential to capture the softening behavior of plain concrete by tension failure due to tensile cracking or compression failure due to slip. The latter is better known as 'bond slip' interfaces which mainly affects the crack spacing. Thereby, the shear slip energy primarily depends upon the mechanical and chemical bond properties in C-S interfaces.

The nonlinear push-over test with interfaces is performed in 2-D and the deformed mesh and load-deflection responses are shown in Figures 21 and 22. Several horizontal cracks develop even in the footing, but the major crack localizes in the first floor wall which agrees with the experimental observations better than the elasto-plastic results of the 3-D simulation shown in Figure 14. In that case, the tensile crack developed at the interface with the wall footing partly because the footing was assumed to remain elastic. The interface damage results agree quite closely with the in-plane ultimate moment capacity of the shear wall obtained from elementary beam theory assuming perfectly plastic behavior of steel and concrete in tension and in compression.

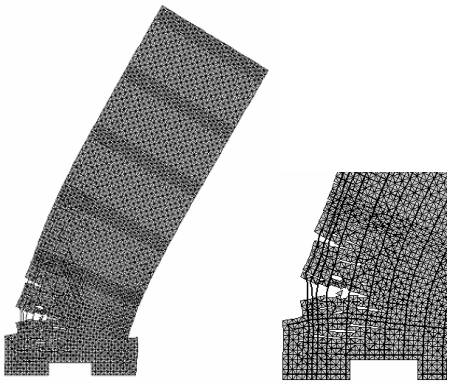

Figure 21. Deformed mesh: In-plane response of interface damage model.

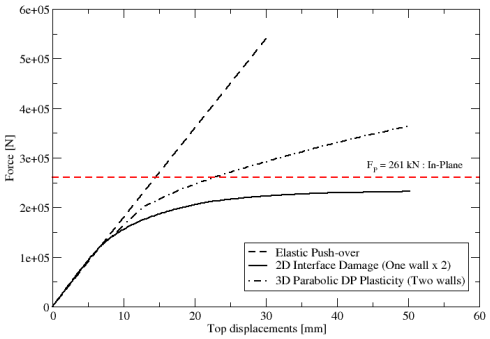

Figure 22. Comparison of in-plane Push-Over response: 3-D plastic and 2-D interface damage models.

7 CONCLUSIONS

The dynamic investigation of a five-story shear-wall structure illustrates the performance and shortcomings of progressive damage simulations under increasing levels of excitation. Additional research is required to examine the interaction of elastic damage and plastic dissipation on hysteretic versus viscous material damping.

8 ACKNOWLEDGEMENTS

The authors wish to acknowledge partial support of this research by the National Science Foundation under grant CMS-0084598.

9 REFERENCES

[1] Mazars, J. et al., 2003, Keynote paper: Numerical modeling for earthquake engineering: the case of lightly RC structural walls, Computational Modelling of Concrete Structures.

[2] Combescure, D. et al., 2002, CAMUS 2000 Benchmark: Experimental results and specifications to the participants, RAPPORT DM2S, Commissariat a l'Energie Atomique.

[3] Willam, K. et al., 2003, Interface Damage Model for Thermomechanical Degradation of Heterogeneous Materials, in press in Special WCCMV Issue on Computational Failure Mechanics, CMAME.